Tree Physiology 27, 1401–1405

Geometrical and physicochemical considerations of the pit membrane in relation to air seeding: the pit membrane as a capillary valve

ARIEL G. MEYRA,[1] VICTOR A. KUZ[1] and GUILLERMO J. ZARRAGOICOECHEA[1–3]

[1] *IFLYSIB (UNLP, CONICET, CICPBA) C.C.565, (B1900BTE) La Plata, Argentina*

[2] *Comisión de Investigaciones Científicas de la Provincia de Buenos Aires, Buenos Aires, Argentina*

[3] *Corresponding author (vasco@iflysib.unlp.edu.ar)*

Received September 18, 2006; accepted February 6, 2007; published online July 3, 2007

Summary A theoretical treatment of some of the factors influencing air seeding at the pit membranes of xylem vessels is given. Pit membrane structure, viewed as a three-dimensional mesh of intercrossing fibrils, and vulnerability to water-stress-induced air seeding are examined in the context of the Young-Laplace equation. Simple geometrical considerations of the porous membrane show that the vapor–liquid interface curvature radius is a function of fiber–fiber distance, fiber radius, wetting angle and position of the wetting line. Air seeding (maximum pressure) occurs at the minimum curvature radius, therefore air seeding is not simply determined by the fiber–fiber distance but is a function of the geometry of the pit membrane and of physicochemical quantities like surface tension and wetting angle. As a consequence of considering a wetting angle different from zero, the minimum curvature radius becomes larger than half the fiber–fiber distance. The present model considers that, for a given pressure difference at the pit membrane, all local interface curvatures are the same. In this sense, pit membranes work as variable capillary valves that allow or prevent air seeding by adjusting local curvatures and interface positions relative to the pore-forming fibers, following the pressure differences across the membranes. The theoretical prediction for the air seeding threshold is consistent with recent experimental data for angiosperm trees.

Keywords: air-seeding pressure, curvature radius, Laplace equation.

Introduction

The ramified anatomy of xylem vessels provides structural support to plants and constitutes the rough topography of the vascular xylem system. Xylem sap, basically water, salt ions, oxygen, inorganic nutrients and organic forms of nitrogen, partially wets the inner xylem vessel walls and the pit membrane (Zimmermann 1983). Sap flows from root to leaves in a xylem vessel in the direction of decreasing pressure (hydrostatic pressure in most plants). Xylem vessels, of millimeter or centimeter length and micrometer cross section, consist of vessel elements joined and connected end to end by a perforation plate (Nobel 1991) and side by side by a number of pits (pit chamber and porous membrane) (Schmid and Machado 1968, Sperry 2000, Choat et al. 2004, Jansen et al. 2004).

A given xylem vessel filled with water is connected laterally by a pit membrane to a neighboring vessel either filled with water or a vapor–air mixture at normal pressure (Jansen et al. 2004). The liquid–vapor interface at the pit membrane ($(1-v)_p$) comprises a group of nanometric regions that can be viewed as curvilinear polygons delimited by cylindrical fibers (Choat et al. 2003, 2004). Each $(1-v)_p$ is characterized by two radii of curvature. By applying classical capillary theory to this geometry, we show how liquid–vapor interfaces at the pit membrane change synchronically with xylem tension and control air-seeding pressures.

Air-seeding at the xylem pit membrane

Recent studies of the xylem pit membrane show that it consists of a mesh with numerous interstitial regions of different geometries (curvilinear polygons) formed by cylindrical fibers of nanometric cross section and nanometric fiber–fiber separation (Choat et al. 2003). The full membrane has a circular shape, consisting of more than one layer of microfibrils usually arranged in three lamellae: two primary walls separated by a middle lamella. A pore through these multiple layers resembles a convoluted tunnel. To analyze the $(1-v)_p$, let us recall the Young-Laplace formula (Landau and Lifshitz 1959, Adamson 1982), which defines a given pressure difference (P_c) as:

$$P_c = \sigma\left(\frac{1}{R_1}+\frac{1}{R_2}\right) \quad (1)$$

with $P_c = P_{at} - P_l$, where P_{at} and P_l are the atmospheric pressure and the xylem liquid tension, respectively, R_1 and R_2 are the principal radii of curvature at any $(1-v)_p$, and σ is the sap surface tension. If $R_1 = R_2 = R_c$ (where R_c is the relevant curvature radius), Equation 1 reduces to $P_c = 2\sigma/R_c$, but if $R_1 = R_c << R_2$, then Equation 1 becomes $P_c = \sigma/R_c$.

A pressure difference moves the $(1-v)_p$ from the first to the last microfibril layer by a dewetting process. In this process, $(1-v)_p$ will have $R_1 \approx R_2$ (the interface is hanging from interwoven microfibrils) or $R_1 < R_2$ (the interface is at the last layer of parallel microfibrils). It follows that, for a given P_c, the first region to cavitate would be the region where $R_1 << R_2$. This is the case for the last layer of parallel microfibrils that is in contact with the liquid-filled vessel. Then Equation 1 reduces to:

$$P_c = \frac{\sigma}{R_c} \tag{2}$$

In Figure 1, we present a possible cross section of the interstitial region when $(1-v)_p$ is at the last layer of microfibrils. From geometrical considerations of Figure 1, it can be shown that the projections of R_c and the fiber radius (R) on the plane defined by the layer are related by $R_c \sin\beta = h_o + R - R\cos\varphi$, where $\beta = \pi/2-(\theta + \varphi)$. Thus, we may write:

$$R_c = \frac{h_o + R(1-\cos\varphi)}{\cos(\theta+\varphi)} \tag{3}$$

where θ is the wetting angle at the three adjoining media (vapor–liquid–fiber), $2h_o$ is the fiber–fiber distance and φ is the angle between a line connecting the two fiber centers and the wetting point. By substituting Equation 3 into Equation 2 we have:

$$P_c = \frac{\sigma\cos(\theta+\varphi)}{h_o + R(1-\cos\varphi)} \tag{4}$$

Shonherr and Bukovac (1972) use a similar expression to study the penetration of stomata by liquids based on a conical capillary model, but in this geometry, the capillary pressure is independent of R. Equation 4 enables calculation of the excess pressure and its maximum value (the air-seeding pressure). If h_o, R, σ and θ are kept constant, then $P_c = f(\varphi)$. The maximum value of P_c is P_{ca} (air-seeding pressure) and it occurs when:

$$\left(\frac{\partial P_c}{\partial \varphi}\right)_{h_o,R,\sigma,\theta} = 0 \tag{5}$$

We also considered the theoretical prediction for the air seeding threshold in the context of some experimental values of σ, θ, R, h_o and P_{ca} published in the literature.

Surface tension In most studies, σ is taken as that of pure water at 20 °C: $\sigma = 72 \times 10^{-3}$ N m^{-1}.

Contact angle The vapor–liquid–fiber contact angle θ has not yet been measured. Pickard (1989), in his analysis of xylem wall contact angle (θ_x), suggested that $0° < \theta_x < 45°$. Recent measurements of θ_x for different species (Zwieniecki and Holbrook 2000, van Ieperen et al. 2001, 2002) show that θ_x varies between 42° and 55°.

Pit membranes are the degraded primary cell walls and middle lamellae of the vessels and are composed of tightly interwoven cellulose microfibrils in a matrix of hemicellulose and pectin polysaccharides (Brett and Waldron 1996, Choat et al. 2003). Pit membrane observations lie near the current edge of X-ray spectroscopy resolution. Boyce et al. (2004) suggest that the chemistry of the compound primary wall within the pit membrane is consistent with that of the primary wall adjacent to the pit, advancing the possibility that θ could be different from zero.

Because θ reflects the magnitude of the vapor–liquid–fiber interaction forces, to assume that $\theta \cong 0°$ (total wetting) implies a low hydraulic conductivity. The viscosity of simple wetting fluids increases by many orders of magnitude when they are confined between solid walls (Derjaguin and Churaev 1985, Bonaccurso et al. 2002), but if the fluid does not wet the solid surface, slippage occurs (Bonaccurso et al. 2002), resulting in greater hydraulic conductivity. Therefore, to assume θ is different from zero not only has implications for the air seeding process but also for transport efficiency. Here, we consider values of θ varying between 0 and 80°. However, effects such as a change in θ due to microfibril roughness or local heterogeneities in the microfibril surface (de Gennes et al. 2003) are not taken into account in the present description.

Fiber–fiber distance Experiments indicate that pit membrane fiber–fiber distances are of the order of 30 nm (Choat et

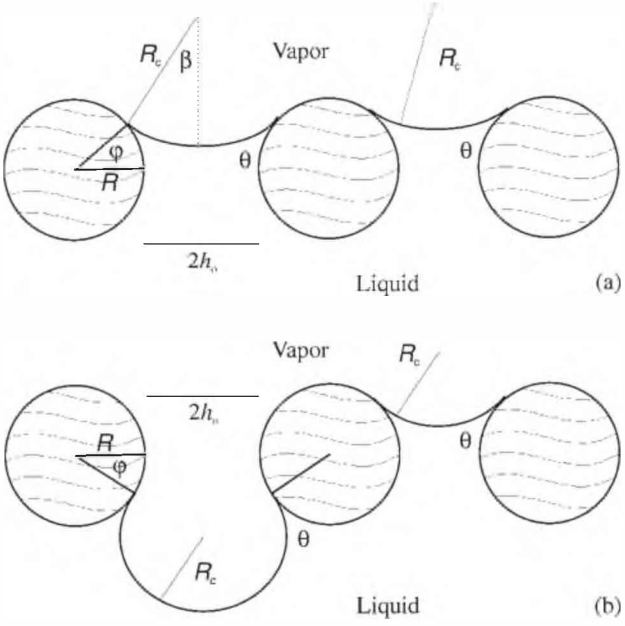

Figure 1. Transverse section of a pit membrane. Abbreviations: R, R_c and $2h_o$ indicate fiber radius, radius of curvature of the liquid–vapor interface at the pit membrane ($(1-v)_p$) and distance between two fibers, respectively. Panels (a) and (b) indicate two possible configurations. The surface separates two contiguous phases: the vapor phase (above) and the tense liquid phase (below). When the vapor pressure increases, R_c decreases, and the system changes from (a) to (b). Configuration (b) depicts the limiting condition for air-seeding at large $2h_o$.

al. 2003). This distance could change as a result of lateral surface tension effects at the wetting line or attraction between fibers.

Fiber radius Estimates of R determined from photographs were taken from the experiments of Choat et al. (2003) and Sperry and Hacke (2004). Although there are no direct measurements of fiber radius, estimates from photographs indicate that fiber radius varies between 20 and 60 nm.

Cavitation pressure Choat et al. (2003) and Sperry and Hacke (2004) studied roots and stem and found variation in cavitation pressures in the range $1 \leq P_{ca} \leq 12$ (MPa). Cochard (2002) measured cavitation pressures in this range by a centrifugal technique. Choat et al. (2004) examined stems of *Fraxinus americana* L. perfused with water ($\sigma = 72$ mN m^{-1}) or with a Triton X solution ($\sigma = 31$ mN m^{-1}) and found cavitation pressures of $P_{ca} = 1.93$ and 1.17 MPa for water and Triton X solution, respectively.

Results

Solving Equation 2 for the experimental cavitation pressures given in the previous section, we find that $R_c = 37.31$ and 26.5 nm for water and Triton X, respectively. With these values of R_c, and with θ and R as input data in the ranges $0° \leq \theta \leq 80°$ and $20 \text{ nm} \leq R \leq 40$ nm, Equations 4 and 5 are solved for h_o and φ. The results are shown in Table 1 for water and Triton X and Figure 2 shows $P_c = P_c(\varphi)$ for these systems. It can also be seen that the maximum values of $P_c(\varphi)$ set up P_{ca}.

Variations in P_{ca} with h_o for different values of R and θ are shown in Figure 3. In this figure, total wetting, $\theta = 0°$ ($R_c = h_o$), is assumed, implying that P_{ca} is independent of R. For small wetting angles ($\theta = 30°$), $P_{ca}(h_o)$ shows a weak dependence on R, but this dependence becomes significant for larger θ.

Discussion

The theoretical predictions for the air seeding threshold, derived from Equations 4 and 5, are consistent with recent experimental data for angiosperm trees. This pit membrane model is also consistent with the fact that, at equilibrium, curvature must be constant over any free surface separation (Landau and Lifshitz 1959). In this sense, a pit membrane is viewed as a variable capillary valve that adjusts its local curvature to inner and outer pressure differences. Each of the multiple nanometric regions that form the liquid–vapor surface of separation in each pit membrane must necessarily have the same curvature, and the intrinsic geometric design is able to respond "instantaneously" to the daily or nocturnal variations in xylem tension by changing each nanometric region of the local curvature. The present explanation of the mechanism of air-seeding in xylem vessels under tension is not only different from previous explanations in the sense that P_{ca} is determined by R and h_o, and by the physicochemical quantities σ and θ, but it also offers a new view of how pit membranes work.

Zimmerman (1983) conducted experimental research to

Table 1. Results from Equations 4 and 5 for *Fraxinus americana* with experimental air seeding pressures of $P_{ca} = 1.93$ and 1.17 MPa for water (a) and Triton X solution (b), respectively (Choat et al. 2004). A range of wetting angle values (θ) (effect of total or partial wetting) and a range of fiber radii (R) values (different fiber radii) are considered as input data. The air-seeding pressure is reached for different values of half the fiber–fiber distance (h_o) and the angle between the line connecting the centers of two fibers and the wetting point (φ) as a function of the input values. For water, $R_c = 37.31$ nm and for Triton X solution, $R_c = 26.50$ nm.

θ (degrees)	R (nm)	φ (degrees)	h_o (nm)
Water			
0	20	0.0	37.31
0	30	0.0	37.31
0	40	0.0	37.31
30	20	–19.48	35.53
30	30	–16.61	35.04
30	40	–14.32	34.68
60	20	–39.53	30.38
60	30	–33.80	28.40
60	40	–28.64	26.96
80	20	–54.43	25.29
80	30	–45.26	21.77
80	40	–38.39	19.24
Triton X			
0	20	0.0	26.50
0	30	0.0	26.50
0	40	0.0	26.50
30	20	–17.18	24.94
30	30	–14.32	24.56
30	40	–12.03	24.32
60	20	–34.38	20.40
60	30	–28.07	18.96
60	40	–23.5	17.92
80	20	–46.41	15.86
80	30	–37.24	13.34
80	40	–30.37	11.67

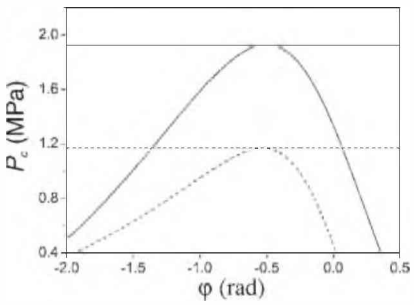

Figure 2. Pressure difference (P_c) as a function of the angle between the line connecting the centers of two fibers and the wetting point (φ) (Equation 4) for *Fraxinus americana* (the solid line denotes water and the dashed line denotes Triton X solution). The maximum values indicate the experimental air-seeding pressures (1.93 MPa for water and 1.17 MPa for Triton X solution) (Choat et al. 2004). We calculated $P_c(\varphi)$ based on wetting angle (θ) = 60°, fiber radius (R) = 40 nm and half the fiber–fiber distance (h_o) = 26.96 nm at $\varphi = -28.65°$ for water, and $\theta = 80°$, $R = 40$ nm and $h_o = 11.67$ nm at $\varphi = -30.37°$ for Triton X solution (see Table 1).

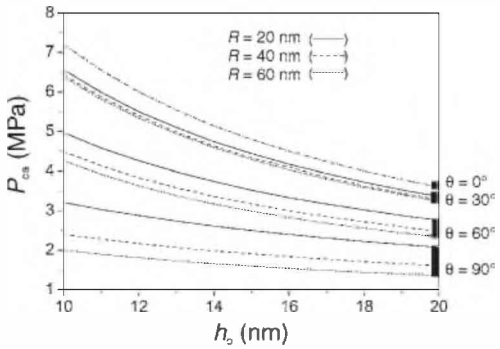

Figure 3. Variation in air seeding pressure (P_{ca}) with half the fiber–fiber distance (h_o) for different values of microfibril radius (R) and wetting angle (θ). The different curves were obtained by substituting Equation 5 in Equation 4 with surface tension (σ) = 72 mN m^{-1}. Black bars on the right indicate the values of angle θ corresponding to different values of R. The curve for $\theta = 0°$ ($R_c = h_o$) is independent of R, where R_c is the radius of curvature.

prove the air-seeding hypothesis. More recently, Choat et al. (2003, 2004) examined pit membrane structure by scanning electron microscopy of suspensions of colloidal gold particles perfused through branch sections, and measured fiber–fiber distance and air-seeding pressures. Although these authors applied a simplified form of the Laplace equation, they did not find correspondence between the fiber–fiber distance and cavitation pressure. In the notation of the present work, they assumed $h_o = R_c$ and $\theta = 0$ (total wetting), that is they neglected the effects of partial wetting (see Table 1). Considering $h_o = R_c$ may be a good approximation for parallel plates, but not for fibers that are wetted parallel to the fiber axes, as happens in the pit membrane. In these kind of valves, fiber curvature changes the $(1-v)_p$ curvature synchronically with the variation in xylem tension or atmospheric pressure (see Figure 1). Equations 4 and 5 account for this and provide not only an explanation for the low values of air-seeding pressures, despite the small pores of typical pit membranes, but also show how the $(1-v)_p$ curvature variation with pressure (different height) in the vascular xylem system depends on both pit membrane design and aging. We have considered that fibers have a cylindrical shape and the same curvature radius (a different fiber radius will not change the present approach), but if the fiber shape is irregular such that the curvature $\kappa = 1/R_c$ varies continuously along the fiber from positive to negative values (i.e., the fiber curvature has a point of inflexion (Lipschutz 1969)), then somewhere in the region close to the inflexion point (depending on the wetting angle) R_c goes to infinity. According to Equation 2, the relationship between P_c and R_c will not be satisfied. In this kind of fiber geometry, when xylem tension increases, R_c also increases and air-seeding could spontaneously occur independently of the fiber–fiber distance.

The present analysis could also be applied to other capillary valves such as the torus-margo of conifer tracheids. In this valve, the impermeable and rough torus surface (Pittermann et al. 2005) blocks sap flow at the pit in proportion to the P_c, and it is able to sustain P_{ca} at the same order or higher than the pit membrane of angiosperms (Hacke et al. 2004). Torus-margo systems have more efficient water discharge than membrane pit valves (Pittermann et al. 2005). Also, the loosely suspended torus in the pit chamber is able to change its relative position with respect to the inner pit wall by changing the radius of curvature of the $(1-v)_t$ synchronically with capillary pressure. The torus $(1-v)_t$ is not symmetric because of roughness of the torus surface and pit wall. At this nanometric scale, P_c follows R_c, which is controlled by the stochastic roughness of both surfaces. Therefore, if there is correspondence between surface roughness and R, and between their mutual distance and h_o, then the torus-margo and pit membrane are equivalent capillary systems because they control P_c and P_{ca} by similar parameters h_o, R, θ and φ.

Previous arguments indicate that variable capillary valves are important not only in allowing air-seeding but also in controlling sap flow. The change in R_c induced by evaporation produces higher excess capillary pressure. In turn this pressure moves the sap from root to stem.

Acknowledgments

This work was partially supported by Universidad Nacional de La Plata, CONICET and CICPBA. G.J.Z. is a member of "Carrera del Investigador Científico" CICPBA.

References

Adamson, A.W. 1982. Physical chemistry of surfaces. John Willey & Sons, New York, 664 p.

Bonaccurso, E., M. Kappl and H.J. Butt. 2002. Hydrodynamics force measurements: boundary slip of water on hydrophilic surfaces and electrokinetic effects. Phys. Rev. Lett. 88:076103.1–076103.4.

Boyce, C.K., M.A. Zwieniecki, G.D. Cody, C. Jacobsen, S. Wirick, A.H. Knoll and M. Holbrook. 2004. Evolution of xylem lignification and hydrogel transport regulation. Proc. Nat. Acad. Sci. USA 101:17,555–17,558.

Brett, C. and K. Waldron. 1996. Physiology and biochemistry of plant cell walls. *In* Topics in Plant Functional Biology. Eds. M. Black and B. Charlwood. Chapman and Hall, London, pp 1–247.

Choat, B., M. Ball, J. Luly and J. Holtum. 2003. Pit membrane porosity and water stress-induced cavitation in four co-existing dry rain forest tree species. Plant Physiol. 131:41–44.

Choat, B., S. Jansen, M.A. Zwieniecki, E. Smets and N.M. Holbrook. 2004. Changes in pit membrane porosity due to deflection and stretching: the role of vestured pits. J. Exp. Bot. 55:1569–1575.

Cochard, H. 2002. A technique for measuring hydraulic conductance under negative pressures. Plant Cell Environ. 25:815–819.

de Gennes, P.G., F.B. Wyart and D. Quere. 2003. Capillarity and wetting phenomena: drops, bubbles, pearls, waves. Springer-Verlag, Berlin, 291 p.

Derjaguin, B.V. and N.V. Churaev. 1985. Properties of layers adjacent to the interfaces. *In* Fluid Interfacial Phenomena. Ed. C.A. Croxton. John Wiley & Sons, New York, 663–738.

Hacke, U.G., J. S. Sperry and J. Pittermann. 2004. Analysis of circular bordered pit function II. Gymnosperm tracheids with torus-margo pit membranes. Am. J. Bot. 91:386–400.

Jansen, S., P. Baas, P. Gasson, F. Lens and E. Smets. 2004. Variation in xylem structure from tropics to tundra: evidence from vestured pits. Proc. Nat. Acad. Sci. USA 101:8833–8837.

Landau, L.D. and E.M. Lifshitz. 1959. Fluid mechanics. Academic Press, New York, 536 p.

Lipschutz, M.M. 1969. Differential geometry. McGraw Hill Book Company, New York, 269 p.

Nobel, P.S. 1991. Physicochemical and environmental plant physiology. Academic Press, San Diego, 635 p.

Pickard, W.F. 1989. How might a tracheary element which is embolized by day be healed by night? J. Theor. Biol. 141:259–279.

Pittermann, J., J.S. Sperry, U.G. Hacke, J.K. Wheeler and E.H. Sikkema. 2005. Torus-margo pits help conifers compete with angiosperms. Science 310:1924.

Schmid, R. and R.D. Machado. 1968. Pit membranes in hardwoods—fine structure and development. Protoplasma 66: 185–204.

Shonherr, J. and M.J. Bukovac. 1972. Penetration of stomata by liquids. Plant Physiol. 49:813–819.

Sperry, J.S. 2000. Hydraulic constraints on plant gas exchange. Agric. For. Meteorol. 104:13–23.

Sperry, J.S. and U.G. Hacke. 2004. Analysis of circular bordered pit function I. Angiosperm vessels with homogenous pit membranes. Am. J. Bot. 91:369–385.

van Ieperen, W., J. Nijsse, C.J. Keijzer and U. Van Meeteren. 2001. Induction of air embolism in xylem conduits of pre-defined diameter. J. Exp. Bot. 52:981–991.

van Ieperen, W., U. van Meeteren and J. Nijsse. 2002. Embolism repair in cut flower stems: a physical approach. Postharv. Biol. Technol. 25:1–14.

Zimmermann, M.H. 1983. Xylem structure and the ascent of sap. Springer-Verlag, Berlin, 143 p.

Zwieniecki, M.A. and N.M. Holbrook. 2000. Bordered pit structure and vessel wall surface properties. Implications for embolism repair. Plant Physiol. 123:1015–1020.